Efficient and Accurate Computation of the Bogoliubov-De Gennes Excitations for the Quasi-2D Dipolar Bose-Einstein Condensates

Yuqing Zhang, Xin Liu and Manting Xie*

Center for Applied Mathematics, Tianjin University, Tianjin 300072, China.

Received 30 November 2020; Accepted (in revised version) 25 February 2021.

Abstract. An efficient spectrally accurate multigrid method for the Bogoliubov-de Gennes excitations of the quasi-2D dipolar Bose-Einstein condensates is proposed. The wave function/eigenmodes are spatially discretised by the Fourier spectral method. The convolution-type nonlocal potential are computed in $\mathcal{O}(N\log(N))$ operations with a spectral accuracy by the kernel truncation method. In addition, the influence of the model parameters on the eigenvalue distribution is studied and for various dipole orientations and an anisotropic external potential the phase diagrams of the eigenmodes are presented. Examples verify the spectral accuracy of the method.

AMS subject classifications: 35Q40, 35Q41, 65M70, 65T40, 65T50

Key words: Bogoliubov-de Gennes excitation, Bose-Einstein condensate, convolution-type nonlocal interaction, spectral method, kernel truncation method.

1. Introduction

The Bose-Einstein condensate (BEC), known as the "fifth state of matter", was theoretically predicted by S. Bose and A. Einstein at the beginning of the last century. Since 1995, the realisation of the BEC of dilute alkalis metal atoms opens up a new direction in the study of ultra-cold atoms [2]. Over the past few years, physicists have been looking for a novel type of quantum gases with dipolar interaction, acting between particles with permanent magnetic or electric dipole moments. It is possible to explore the dipolar BEC of ultra-cold atomic in experiments due to the remarkable discovery of ^{52}Cr atoms in 2005 [26]. A dipolar BEC with ^{164}Dy atoms, whose dipole-dipole interaction (DDI) is much stronger than that of ^{52}Cr, was achieved in experiments in 2011 [32]. In 2012, a new dipolar BEC of ^{168}Er atoms has been realised at the Insbruck University [1]. These experiments show that apart from early BECs, the DDI of dipolar BEC is anisotropic and long-range ones and

*Corresponding author. *Email addresses:* zyqmath2020@163.com (Y. Zhang), liuxin_0921@163.com (X. Liu), xiemanting@lsec.cc.ac.cn (M. Xie)

this produces some unique phenomena. All of these have greatly promoted the theoretical and numerical investigations of dipolar BECs.

If the temperature T is much lower than a critical temperature T_c, the evolution of quasi-2D dipolar BEC is described by a macroscopic wave function $\psi = \psi(\mathbf{x}, t)$, which satisfies the 2D Gross-Pitaevskii equation (GPE) with DDI term [7, 9, 43]

$$i\partial_t \psi(\mathbf{x}, t) = \left[-\frac{1}{2}\Delta + V(\mathbf{x}) + \beta|\psi|^2 + \lambda\Phi(\mathbf{x}, t)\right]\psi(\mathbf{x}, t), \quad \mathbf{x} \in \mathbb{R}^2, \quad t > 0, \tag{1.1}$$

$$\Phi(\mathbf{x}, t) = \left(U * |\psi|^2\right) = \int_{\mathbb{R}^2} U(\mathbf{x} - \mathbf{x}')\rho(\mathbf{x}')d\mathbf{x}', \qquad \mathbf{x} \in \mathbb{R}^2, \quad t \geq 0 \tag{1.2}$$

with the initial data

$$\psi(\mathbf{x}, t = 0) = \psi_0(\mathbf{x}), \quad \mathbf{x} \in \mathbb{R}^2. \tag{1.3}$$

Here, $\mathbf{x} = (x, y)^T \in \mathbb{R}^2$, t is the time, $\rho(\mathbf{x}, t) := |\psi(\mathbf{x}, t)|^2$ the density, β a dimensionless interaction constant (positive for repulsive interaction and negative for attractive interaction), and $\Phi(\mathbf{x}, t)$ is the real-valued nonlocal (long-range) DDI defined as the convolution of the interaction kernel $U(\mathbf{x})$ and a density function ρ. Besides, $V(\mathbf{x})$ is a given real-valued external trapping potential determined by the type of the system under consideration. In most of the BEC experiments, the harmonic potential $V(\mathbf{x})$ is chosen to trap the condensate — i.e.

$$V(\mathbf{x}) = \frac{1}{2}\left(\gamma_x^2 x^2 + \gamma_y^2 y^2\right),$$

where $\gamma_x > 0$ and $\gamma_y > 0$ are dimensionless constants proportional to the trapping frequencies in x- and y-directions, respectively. Moreover, λ is a constant characterising the strength of DDI and $U(\mathbf{x})$ is a long-range DDI potential. Here, $U(\mathbf{x})$ has the form

$$U(\mathbf{x}) = -\frac{3}{2}\left(\partial_{\mathbf{n}_\perp\mathbf{n}_\perp} - n_3^2\nabla_\perp^2\right)\frac{1}{(2\pi)^{3/2}}\int_{\mathbb{R}^2}\frac{e^{-s^2/2}}{\sqrt{|\mathbf{x}|^2 + \epsilon^2 s^2}}\mathrm{d}s, \quad \mathbf{x} \in \mathbb{R}^2 \tag{1.4}$$

with a given unit vector $\mathbf{n} = (n_1, n_2, n_3)^T$, i.e. $\|\mathbf{n}\|_{l^2} = \sqrt{n_1^2 + n_2^2 + n_3^2} = 1$, representing the 3D dipole axis [7], and

$$\nabla_\perp = (\partial_x, \partial_y)^T, \quad \mathbf{n}_\perp = (n_1, n_2)^T, \quad \partial_{\mathbf{n}_\perp} = \mathbf{n}_\perp \cdot \nabla_\perp, \quad \partial_{\mathbf{n}_\perp\mathbf{n}_\perp} = \partial_{\mathbf{n}_\perp}(\partial_{\mathbf{n}_\perp}).$$

As the confinement gets stronger and by a formal analysis — c.f. Refs. [9, 21], we have

$$U \to U^\infty(\mathbf{x}) := -\frac{3}{2}\left(\partial_{\mathbf{n}_\perp\mathbf{n}_\perp} - n_3^2\nabla_\perp^2\right)\frac{1}{2\pi}\frac{1}{|\mathbf{x}|}, \quad \text{as} \quad \epsilon \to 0. \tag{1.5}$$

The quasi-2D GPE (1.1)-(1.3) conserves two important quantities — viz. the total mass (or normalisation) of the wave function

$$N\big(\psi(\mathbf{x}, t)\big) := \|\psi(\mathbf{x}, t)\|^2 = \int_{\mathbb{R}^2}|\psi(\mathbf{x}, t)|^2\mathrm{d}\mathbf{x} \equiv N\big(\psi(\mathbf{x}, 0)\big)$$

and the energy per particle

$$E\big(\psi(\mathbf{x},t)\big) := \int_{\mathbb{R}^2}\left[\frac{1}{2}|\nabla\psi(\mathbf{x},t)|^2 + V(\mathbf{x})|\psi(\mathbf{x},t)|^2 + \frac{\beta}{2}|\psi(\mathbf{x},t)|^4 + \frac{\lambda}{2}\Phi(\mathbf{x},t)|\psi(\mathbf{x},t)|^2\right]\mathrm{d}\mathbf{x}$$
$$\equiv E\big(\psi(\mathbf{x},0)\big), \quad t \geq 0.$$

In order to study the steady-state solution $\phi_s(\mathbf{x})$ by the ansatz function $\psi(\mathbf{x},t) = e^{i\mu t} \times \phi_s(\mathbf{x})$, the 2D GPE (1.1)-(1.3) can be formally reduced to the following nonlinear eigenvalue problem:

$$\mu_s\phi_s(\mathbf{x}) = \left[-\frac{1}{2}\Delta + V(\mathbf{x}) + \beta|\phi_s(\mathbf{x})|^2 + \lambda\,\Phi_s(\mathbf{x})\right]\phi_s(\mathbf{x}), \tag{1.6}$$

where μ_s is the chemical potential, $\phi_s(\mathbf{x})$ the time-independent wave function and $\Phi_s(\mathbf{x}) = U * |\phi_s|^2$. Its eigenvalue (or the chemical potential) μ_s can be computed from the corresponding eigenfunction ϕ_s as

$$\mu_s = \int_{\mathbb{R}^2}\left[\frac{1}{2}|\nabla\phi_s(\mathbf{x})|^2 + V(\mathbf{x})|\phi_s(\mathbf{x})|^2 + \beta|\phi_s(\mathbf{x})|^4 + \lambda\Phi_s(\mathbf{x})|\phi_s(\mathbf{x})|^2\right]\mathrm{d}\mathbf{x}$$
$$= E(\phi_s) + \frac{1}{2}\int_{\mathbb{R}^2}\left[\beta|\phi_s(\mathbf{x})|^4 + \lambda\Phi_s(\mathbf{x})|\phi_s(\mathbf{x})|^2\right]\mathrm{d}\mathbf{x}.$$

The ground state $\phi_g(\mathbf{x})$ of BEC is defined as the minimizer of the following non-convex minimization problems as follows:

$$\phi_g(\mathbf{x}) = \operatorname*{argmin}_{\phi\in\mathscr{S}} E(\phi),$$

where

$$\mathscr{S} := \left\{\phi(\mathbf{x}) \mid \|\phi\|^2 := \int_{\mathbb{R}^2}|\phi(\mathbf{x})|^2 d\mathbf{x} = 1,\ E(\phi) < \infty\right\}.$$

Moreover, the ground state is a one stationary state with the lowest energy. Nowadays, there are various studies of the ground state [3,4,7–9,13,30,31,38,42,44] and the dynamics of dipolar BECs [12,15,28,34].

It is well known, that GPE can be used to accurately describe BECs at the mean field level [22]. On the other hand, GPE does not accurately describe the fluctuations of the BEC [27]. In order to capture the multi-body effects of interatomic interactions, we first need to study the collective excitations beyond GPE. The collective excitation behavior of interacting Boson systems can be explained by the fundamental excitation of the system controlled by quasi-2D GPE (1.1)-(1.3). When excitation is weak and quantum depleted, the collective behavior of the interacting Boson gases can be explained by elementary excitations of the systems governed by GPE (1.1)-(1.3). This phenomenon can be better described by the Bogoliubov-de Gennes (BdG) excitations [5,16,29,33]. Nowadays, the works on elementary excitations in BECs are mainly composed of the GPE for the condensed

part of trapped atom cloud and of BdG excitations for the non-condensed part [27]. In order to present BdG excitations, we assume that the evolution of GPE (1.1)-(1.3) is located around the stationary state ϕ_s with a chemical potential μ_s. Then we represent the wave function as

$$\psi(\mathbf{x},t)=e^{-i\mu t}\Big(\phi_g(\mathbf{x})+\delta\big(u(\mathbf{x})e^{-i\omega t}+\overline{v}(\mathbf{x})e^{i\omega t}\big)\Big),\quad \mathbf{x}=(x,y)^T\in\mathbb{R}^2, \tag{1.7}$$

where $\overline{\xi}$ is the complex conjugate of ξ, $0<\delta\ll 1$ a small quantity used to control the population of quasiparticle excitation, $(u,\overline{v})$ are the modes of the excitations, and ω the corresponding frequency — cf. [23,35]. Here the mode functions are normalised as

$$\int_{\mathbb{R}^2}\big(|u(\mathbf{x})|^2-|v(\mathbf{x})|^2\big)\,\mathrm{d}\mathbf{x}=1. \tag{1.8}$$

Substituting (1.7) into (1.1)-(1.3), collecting the linear terms in δ and evolving in time like $e^{-i\omega t}$ and $e^{i\omega t}$, we arrive at the following BdG equations:

$$\mathscr{L}_{\mathrm{GP}}u+\beta|\phi_s|^2u+\beta\phi_s^2v+\lambda U*\big(\bar{\phi}_s u+\phi_s v\big)\phi_s=\omega u, \tag{1.9}$$

$$\mathscr{L}_{\mathrm{GP}}v+\beta(\overline{\phi}_s)^2u+\beta|\phi_s|^2v+\lambda U*\big(\bar{\phi}_s u+\phi_s v\big)\bar{\phi}_s=-\omega v, \tag{1.10}$$

where ω is the frequency, (u,v) the corresponding eigenvector, and

$$\mathscr{L}_{\mathrm{GP}}:=-\frac{1}{2}\Delta+V(\mathbf{x})+\beta|\phi_s|^2+\lambda\Phi_s-\mu_s.$$

The system (1.9)-(1.10) can be written in the matrix form

$$\begin{pmatrix}\mathscr{A} & \mathscr{B}\\ -\mathscr{A}^* & -\mathscr{B}^*\end{pmatrix}\begin{pmatrix}u\\ v\end{pmatrix}=\omega\begin{pmatrix}u\\ v\end{pmatrix}, \tag{1.11}$$

where

$$\mathscr{A}=\mathscr{L}_{\mathrm{GP}}+\beta\,|\phi_s|^2+\lambda\widehat{\chi}_1,\quad \mathscr{B}=\beta\phi_s^2+\lambda\,\widehat{\chi}_2,$$

and $\mathscr{A}^*$ and $\mathscr{B}^*$ are the adjoints of the operators $\mathscr{A}$ and $\mathscr{B}$, respectively. The operators $\widehat{\chi}_1$ and $\widehat{\chi}_2$ are defined as follows:

$$\big[\widehat{\chi}_1(\xi)\big](\mathbf{x}):=\phi_s(\mathbf{x})\big[U*(\bar{\phi}_s\xi)\big](\mathbf{x})=\phi_s(\mathbf{x})\int_{\mathbb{R}^2}U(\mathbf{x}-\mathbf{x}')\bar{\phi}_s(\mathbf{x}')\xi(\mathbf{x}')\mathrm{d}\mathbf{x}', \tag{1.12}$$

$$\big[\widehat{\chi}_2(\xi)\big](\mathbf{x}):=\phi_s(\mathbf{x})[U*(\phi_s\xi)](\mathbf{x})=\phi_s(\mathbf{x})\int_{\mathbb{R}^2}U(\mathbf{x}-\mathbf{x}')\phi_s(\mathbf{x}')\xi(\mathbf{x}')\mathrm{d}\mathbf{x}'. \tag{1.13}$$

It is worth noting that GPEs are much better studied than BdG equations. Physicists are concerned with analytical solutions of BdG [27,39]. Since the solution of BdG equations is based on accurate evaluation of steady-state BECs, numerical approaches to BdG, especially in the case of dipolar BECs, require substantial efforts. In particular, Ronen *et al.* [35,41] incorporated the Hankel transform in a fast and accurate numerical algorithm to solve BdG

equations. LAPACK and ARPACK libraries can be applied to the BdG equations discretised by finite element/difference methods [18,20,29]. Gao and Cai [23] investigated analytical properties of BdG equations for BEC and proposed numerical methods for their solution.

For BdG equations of the quasi-2D dipolar BEC (1.1)-(1.3), we first have to determine an accurate stationary/ground state solution of a quasi-2D dipolar BEC. However, the nonlocality and anisotropy of the DDI term create substantial difficulties in the evaluation of evaluation of nonlocal potentials. Nevertheless, nowadays there are efficient methods to solve stationary/ground state of dipolar BECs such as non-uniform fast Fourier transform (NUFFT) [13] and preconditioned conjugated gradient (PCG) with kernel truncation method (KTM) [4]. In order to find solutions of the BdG equation (1.11), one has to be able to efficiently evaluate the corresponding operator-functions and solve non-Hermitian operator matrix eigenvalue problems. In particular, the operator-function evaluation requires the fast computation of $\widehat{\chi}_j(\xi)$ defined by a convolution and multiplication — cf. (1.12)-(1.13), with a smooth and fast-decaying function $\xi(\mathbf{x})$. Moreover, it is also the most time-consuming part, which often bottlenecks the entire simulation process because of the absence of fast algorithms, especially, in high dimensional cases. Besides, since the coefficient matrix discretised by a spectral method is large, dense and nonsymmetric, it is not possible to directly store it.

In this paper, we first use the PCG method to compute the ground states of quasi-2D dipolar BECs via KTM for DDI evaluation — cf. [40] with a spectral method for the spatial discretisation. After that, a KTM is employed in order to determine the nonlocal interaction $\widehat{\chi}_j(\xi)$ in (1.12)-(1.13). The large-scale, dense and nonsymmetric discrete BdG equations can be solved by a matrix-free version of the implicitly restarted Arnoldi method (IRAM) [37] such as `eigs` function in MATLAB and ARPACK. Based on the KTM method and matrix-free version of the IRAM, we construct an efficient multigrid method for the eigenvalue problem (2.9). Extensive numerical results demonstrate the efficiency and accuracy of the numerical approach used.

This paper is organised as follows. In Section 2, analytical properties of BdGs are discussed. Section 3 introduces the Fourier spectral method for spatial discretisation, the KTM for the convolution evaluation and a multigrid method for eigenvalue problems. In Section 4, numerical tests are carried out to show the accuracy and efficiency of the numerical methods and to investigate the phase diagram of BdG excitations. Finally, some conclusions are drawn in Section 5.

2. Analytical Properties of BdG Equations

In this section, we show properties of BdG equations (1.9)-(1.10).

Lemma 2.1. *If $\{(u,v),\omega\}$ is a solution of the Eqs.* (1.9)-(1.10)*, then so is $\{(\bar{v},\bar{u}),-\omega\}$. Besides, if u,v satisfy the normalisation constraint* (1.8)*, then the eigenfrequency ω is real.*

Proof. Taking the complex conjugates of the Eqs. (1.9)-(1.10) gives

$$\mathscr{L}_{\mathrm{GP}}\bar{u}+\beta(\bar{\phi}_s)^2\bar{v}+\beta|\phi_s|^2\bar{u}+\lambda\, U*(\bar{\phi}_s\bar{v}+\phi_s\bar{u})\bar{\phi}_s=\omega\bar{u},$$

$$\mathscr{L}_{\rm GP}\bar{v}+\beta|\phi_s|^2\bar{v}+\beta\phi_s^2\bar{u}+\lambda U*(\bar{\phi}_s\bar{v}+\phi_s\bar{u})\phi_s=-\omega\bar{v},$$

which immediately implies $\{(\bar{v},\bar{u}),-\omega\}$ is also a solution.

Multiplying (1.9)-(1.10) respectively by $\bar{u}$ and $\bar{v}$, integrating over $\mathbb{R}^d$ and combining the resulted equations yield

$$\begin{aligned}&\omega\int_{\mathbb{R}^d}\left(|u(\mathbf{x})|^2-|v(\mathbf{x})|^2\right)d\mathbf{x}\\&=\int_{\mathbb{R}^d}\Big\{\frac{1}{2}\left(|\nabla u(\mathbf{x})|^2+|\nabla v(\mathbf{x})|^2\right)+\left(V+2\beta|\phi_s|^2+\lambda\Phi_s-\mu_s\right)\left(|u(\mathbf{x})|^2+|v(\mathbf{x})|^2\right)\\&\qquad+\beta\left(\phi_s^2\bar{u}v+\bar{\phi}_s^2u\bar{v}\right)+\lambda\Big[\bar{u}\widehat{\chi}_1(u)+\bar{v}\widehat{\chi}_1^*(v)+\bar{u}\widehat{\chi}_2(v)+\bar{v}\widehat{\chi}_2^*(u)\Big]\Big\}\mathrm{d}\mathbf{x}.\end{aligned}\tag{2.1}$$

It is clear that the right-hand side of (2.1) is real and hence substitute Eq. (2.1) from its conjugate, we arrive at the identity

$$(\omega-\bar{\omega})\int_{\mathbb{R}^2}\left(|u(\mathbf{x})|^2-|v(\mathbf{x})|^2\right)\mathrm{d}\mathbf{x}=0.$$

Combining it with the normalisation constraint (1.8) shows that ω is also real. □

In the context of elementary excitations for BECs, we consider the BdG equations (1.9)-(1.10) under the condition (1.8) linearised around the ground state ϕ_g. In order to reduce the large scale of (1.11), we use variables change

$$u=f+g,\quad v=f-g.\tag{2.2}$$

For real-valued stationary state ϕ_s, all nonlocal operators are identical — i.e.

$$\widehat{\chi}_1=\widehat{\chi}_2,\quad \mathscr{A}=\mathscr{A}^*,\quad \mathscr{B}=\mathscr{B}^*.$$

Then the BdG equations (1.11) can be written as

$$\begin{pmatrix}0&\mathscr{H}_-\\\mathscr{H}_+&0\end{pmatrix}\begin{pmatrix}f\\g\end{pmatrix}=\omega\begin{pmatrix}f\\g\end{pmatrix},\tag{2.3}$$

where

$$\mathscr{H}_-=\mathscr{L}_{\rm GP}=-\frac{1}{2}\Delta+V(\mathbf{x})+\beta|\phi_s|^2-\mu_s+\lambda\Phi_s,\tag{2.4}$$

$$\mathscr{H}_+=\mathscr{L}_{\rm GP}+2\beta|\phi_s|^2+2\lambda\widehat{\chi}_1=-\frac{1}{2}\Delta+V(\mathbf{x})+3\beta|\phi_s|^2-\mu_s+\lambda\Phi_s+2\lambda\widehat{\chi}_1.\tag{2.5}$$

Correspondingly, the original constraint (1.8) takes the form

$$\Re\left(\int_{\mathbb{R}^2}\left(f(\mathbf{x})g^*(\mathbf{x})\right)\mathrm{d}\mathbf{x}\right)=\frac{1}{4},\tag{2.6}$$

where $\Re$ refers to the real part of the corresponding expression. Hence, we have

$$\mathscr{H}_+ f = \omega g, \tag{2.7}$$
$$\mathscr{H}_- g = \omega f. \tag{2.8}$$

From (2.7) and (2.8), the eigenvalue problem (2.3) can be transformed to one of the product eigenvalue problems — viz.

$$\mathscr{H}_-\mathscr{H}_+ f = \omega^2 f, \tag{2.9}$$
$$\mathscr{H}_+\mathscr{H}_- g = \omega^2 g. \tag{2.10}$$

Here, we focus on solving the eigenvalue problem (2.9) under the constraint (2.6). It is worth noting that the coefficient operators $\mathscr{H}_-\mathscr{H}_+$ in (2.9) and $\mathscr{H}_+\mathscr{H}_-$ in (2.10) are also non-selfadjoint.

Lemma 2.2. *Let V be the harmonic potential*

$$V(\boldsymbol{x}) = \frac{1}{2}\sum_{\alpha}\gamma_\alpha^2\alpha^2$$

with $\alpha = x$ or $\alpha = y$. If the stationary state ϕ_s is real-valued, then there exist Bogoliubov eigenvalues $\omega_\alpha = \gamma_\alpha$ and the associated eigenfunctions

$$u_\alpha = \frac{1}{\sqrt{2}}\left(\gamma_\alpha^{-\frac{1}{2}}\partial_\alpha\phi_s - \gamma_\alpha^{\frac{1}{2}}\alpha\phi_s\right), \quad v_\alpha = \frac{1}{\sqrt{2}}\left(\gamma_\alpha^{-\frac{1}{2}}\partial_\alpha\phi_s + \gamma_\alpha^{\frac{1}{2}}\alpha\phi_s\right).$$

Proof. We only consider the case $\alpha = x$. The other one can be proved analogously. Since the situations $\beta = 0$ or $\lambda = 0$ can be easily handled, we focus on the cases $\beta \neq 0$ and $\lambda \neq 0$. It is well known that the steady state ϕ_s satisfies the Euler-Lagrange equation

$$\mu_s\phi_s(\mathbf{x}) = \left[-\frac{1}{2}\Delta + V + \beta|\phi_s|^2 + \lambda\Phi_s(\mathbf{x})\right]\phi_s(\mathbf{x}), \quad \|\phi_s\| = 1. \tag{2.11}$$

Computing the first derivative of the Eq. (2.11) in x gives

$$\mathscr{H}_+(-\partial_x\phi_s) = \left(-\frac{1}{2}\Delta + V + 3\beta|\phi_s|^2 + \lambda\Phi_s + 2\lambda\widehat{\chi}_1 - \mu_s\right)(-\partial_x\phi_s) = \gamma_x^2 x\phi_s. \tag{2.12}$$

Multiplying this equation by $\gamma_x x$ yields

$$\mathscr{H}_-(\gamma_x x\phi_s) = \left(-\frac{1}{2}\Delta + V + \beta|\phi_s|^2 + \lambda\Phi_s - \mu_s\right)(\gamma_x x\phi_s) = -\gamma_x\partial_x\phi_s. \tag{2.13}$$

It follows that $(-\partial_x\phi_s, \gamma_x x\phi_s)$ solves (2.7) and (2.8) with $\omega = \gamma_x$. Observing that

$$-\int_{\mathbb{R}^2}\gamma_x x\partial_x\phi_s\phi_s\mathrm{d}x\mathrm{d}y = \frac{\gamma_x}{2},$$

we obtain that the functions

$$f = \frac{1}{\sqrt{2}}\gamma_x^{-\frac{1}{2}}\partial_x\phi_s, \quad g = -\frac{1}{\sqrt{2}}\gamma_x^{\frac{1}{2}}x\phi_s$$

satisfy the Eqs. (2.7) and (2.8) with the eigenvalue $\omega = \gamma_x$. It follows from the variables change (2.2) that

$$(u_x, v_x) = \left(\frac{1}{\sqrt{2}}\left(\gamma_x^{-\frac{1}{2}}\partial_x\phi_s - \gamma_x^{\frac{1}{2}}x\phi_s\right), \frac{1}{\sqrt{2}}\left(\gamma_x^{-\frac{1}{2}}\partial_x\phi_s + \gamma_x^{\frac{1}{2}}x\phi_s\right)\right),$$

where $\omega = \gamma_x$ with respect to x, is an analytic solution of BdG equation (1.9)-(1.10). □

3. Numerical Algorithms for BdG Equations

In this section, we present numerical algorithms, including the Fourier spectral discretisation, KTM for nonlocal interaction and a multigrid method.

3.1. Fourier spectral discretisation

Due to the external trapping potential $V(\mathbf{x})$, the solution of the dipolar GPE (1.1)-(1.3) decays exponentially fast at the far-field, and so is the solution of the BdG equation (1.9)-(1.10). It is reasonable to assume that the stationary state ϕ_s and the eigenfunction (u, v) are smooth and decay rapidly. Usually we first truncate the space $\mathbb{R}^2$ into a sufficiently large rectangular domain $\Omega := [-L, L]^2$ such that the truncation error is negligible and impose periodic boundary conditions for the wave function ϕ_s and the eigenfunctions (u, v). Since the long-range nonlocal DDI Φ_s and the convolution part of $\widehat{\chi}_j(\xi)$ given by (1.4) and (1.12)-(1.13), decay polynomially fast at the far field, it is natural not to prescribe any boundary condition but to directly evaluate the convolutions. Note that it is challenging to efficiently compute such convolutions with a spectral accuracy.

By using Fourier spectral method [7,9] for the discretisation of (2.9), we obtain a linear algebraic system in the matrix form — viz.

$$H_h^- H_h^+ f^h = (\omega^h)^2 f^h, \tag{3.1}$$

where $H_h^- = H_{h,1} + H_{h,2} + H_{h,3}$ and $H_h^+ = H_{h,1} + \widetilde{H}_{h,2} + H_{h,3} + H_{h,4}$ are, respectively, the matrices of the discrete operators for $\mathscr{H}_+$ and $\mathscr{H}_-$ in (2.9). We note that $H_{h,1}, H_{h,2}, \widetilde{H}_{h,2}$, $H_{h,3}$ and $H_{h,4}$ are the discretisation matrices of $-\frac{1}{2}\Delta$, $V(\mathbf{x})+\beta|\phi_s|^2-\mu_s$, $V(\mathbf{x})+3\beta|\phi_s|^2-\mu_s$, $\lambda\Phi_s$ and $2\lambda\widehat{\chi}_1$ in (2.4)-(2.5), respectively, and (f^h, g^h) is the discrete vector for (f, g).

The Fourier spectral method can be briefly described as follows. The domain Ω is discretised by a mesh of size h, and the mesh grid is $\mathscr{T}_h = \{(x_p, y_q)\}_{(p,q)\in\Lambda}$ with $\Lambda = \{(p,q)|p = 0, 1, \ldots, N-1, q = 0, 1, \ldots, N-1\}$. Take symmetric and uniform interval discrete with L. Then $x_p = -L + ph, y_q = -L + qh, h = 2L/N$ with $p, q = 0, 1, \ldots, N-1$. The wave function ψ, the derivatives of ψ, and the Laplacian of ψ are well approximated by the discrete fast

Fourier transform (FFT). The Fourier pseudo-spectral approximation for function $\xi(x,y)$ with periodic boundary conditions can be written as

$$\xi(x,y) \approx \frac{1}{N^2} \sum_{k=-\frac{N}{2}}^{\frac{N}{2}-1} \sum_{l=-\frac{N}{2}}^{\frac{N}{2}-1} \widehat{\xi}_{kl} e^{\frac{ik\pi}{L}(x+L)} e^{\frac{il\pi}{L}(y+L)}$$

with the discrete Fourier transforms coefficients

$$\widehat{\xi}_{kl} = \sum_{p=0}^{N-1} \sum_{q=0}^{N-1} \xi_{pq} e^{-\frac{ik\pi}{L}(x_p+L)} e^{-\frac{il\pi}{L}(y_q+L)}, \quad k,l = -N/2,\ldots,-1,0,1,\ldots,N/2-1,$$

where $\xi_{pq} := \xi(x_p, y_q)$, $p,q = 0,1,\ldots,N-1$. According to the Fourier spectral discretisation we have

$$\partial_{xx}\xi(x,y) \approx \frac{1}{N^2} \sum_{k=-\frac{N}{2}}^{\frac{N}{2}-1} \sum_{l=-\frac{N}{2}}^{\frac{N}{2}-1} \left(\frac{ik\pi}{L}\right)^2 \widehat{\xi}_{kl} e^{\frac{ik\pi}{L}(x+L)} e^{\frac{il\pi}{L}(y+L)},$$

$$\partial_{yy}\xi(x,y) \approx \frac{1}{N^2} \sum_{k=-\frac{N}{2}}^{\frac{N}{2}-1} \sum_{l=-\frac{N}{2}}^{\frac{N}{2}-1} \left(\frac{il\pi}{L}\right)^2 \widehat{\xi}_{kl} e^{\frac{ik\pi}{L}(x+L)} e^{\frac{il\pi}{L}(y+L)},$$

so that the approximation of the second order derivative $(\partial_{xx} + \partial_{yy})\xi(x,y)$ at the grid points (x_p, y_q), $p,q = 0,1,\ldots,N-1$ is

$$(\partial_{xx} + \partial_{yy})\xi(x,y) \approx \frac{1}{N^2} \sum_{k=-\frac{N}{2}}^{\frac{N}{2}-1} \sum_{l=-\frac{N}{2}}^{\frac{N}{2}-1} \left(\frac{i\pi}{L}\right)^2 \left(k^2+l^2\right) \widehat{\xi}_{kl} e^{\frac{ik\pi}{L}(x+L)} e^{\frac{il\pi}{L}(y+L)}.$$

It is easy to determine $H_{h,1}$. Since $H_{h,2}$ and $\widetilde{H}_{h,2}$ are multiplication operators in the physical space, their operations on f_h are easily accessed by the point-wise multiplication. Since the nonlocal interaction $\widehat{\chi}_j(\xi)$ consists of convolution and multiplication. Therefore, it is not diagonalisable in either phase or physical space. Efficient and accurate evaluation of $\widehat{\chi}_j(\xi)$ represents a challenging problem. However, it can be handled with a spectral accuracy by the KTM [4, 40] considered in the next subsection.

3.2. KTM for DDI and nonlocal interaction evaluation

Given a smooth and fast-decaying density $\rho(\mathbf{x})$, we introduce KTM for the following nonlocal convolution:

$$\begin{aligned}\varphi &= \left(\frac{1}{(2\pi)^{3/2}} \int_{\mathbb{R}} \frac{e^{-s^2/2}}{\sqrt{|\mathbf{x}|^2+\epsilon^2 s^2}} \mathrm{d}s\right) * \left(-\frac{3}{2}\left(\partial_{\mathbf{n}_\perp \mathbf{n}_\perp} - n_3^2 \nabla_\perp^2\right)\rho\right) \\ &=: \widetilde{U} * \widetilde{\rho}.\end{aligned}$$

For simplicity, below we omit the tilde in the symbols of $\widetilde{U}$ and $\widetilde{\rho}$. Since the density ρ is compactly supported in Ω, we have

$$\varphi(\mathbf{x}) = \int_{\mathbb{R}^2} U(\mathbf{x}-\mathbf{x}')\rho(\mathbf{x}')\mathrm{d}\mathbf{x}' = \int_{\Omega} U(\mathbf{x}-\mathbf{x}')\rho(\mathbf{x}')\mathrm{d}\mathbf{x}'. \tag{3.2}$$

In order to compute φ over Ω, we cut off the interaction outside a larger domain, which is usually chosen as a ball $\mathbf{B}_G := \{\mathbf{x}||\mathbf{x}| < G\}$ with the radius G superior to the diameter of Ω. Setting $U(\mathbf{x}) = 0$ for all $\mathbf{x} \in \mathbb{R}^2 \backslash \mathbf{B}_G$, noticing that $\mathbf{x}-\mathbf{x}' \in \mathbf{B}_G$ for any $\mathbf{x}, \mathbf{x}' \in \Omega$ and combining it with (3.2) yield

$$\varphi(\mathbf{x}) = \int_{\mathbb{R}^2} U_G(\mathbf{x}-\mathbf{x}')\rho(\mathbf{x}')\mathrm{d}\mathbf{x}' = \frac{1}{(2\pi)^2}\int_{\mathbb{R}^2} \widehat{U}_G(\mathbf{k})\widehat{\rho}(\mathbf{k})e^{i\mathbf{k}\cdot\mathbf{x}}\mathrm{d}\mathbf{k}, \quad \mathbf{x} \in \Omega, \tag{3.3}$$

where $U_G(\mathbf{x}) = U(\mathbf{x})\zeta_{\mathbf{B}_G}(\mathbf{x})$ and $\zeta_{\mathbf{B}_G}(\mathbf{x})$ is the characteristic function on the ball $\mathbf{B}_G$. Now we apply the trapezoidal quadrature to the modified Fourier integral whose integrand is not singular any more [4].

It has to be mentioned that the Fourier transform of a 2D truncated kernel U_G can be written as

$$\widehat{U}_G(\mathbf{k}) = 2\pi \int_0^G J_0(kr)U(r)dr, \tag{3.4}$$

where $k = |\mathbf{k}|$, $r = |\mathbf{x}|$ and J_0 is the first-kind Bessel functions with index 0 [25]. The integral can be evaluated via adaptive Gauss-Kronrod quadrature numerically with a desired accuracy (3.4).

In this work, we consider the square domain $\Omega = [-L, L]^2$ and set $G \geq 2\sqrt{2}L$. This suggests that a threefold zero-padding of the density in each spatial direction is sufficient to guarantee spectral accuracy. It is known that a twofold zero-padding is sufficient with a precomputation from [40]. We can use the Fourier spectral method to compute ρ. Let $\bar{\rho}_{pq}$ refer to the zero-padding by a factor of S, i.e.

$$\bar{\rho}_{pq} = \begin{cases} \rho_{pq}, & p = \dfrac{S-1}{2}N_x, \ldots, \dfrac{S+1}{2}N_x - 1 \quad \text{and} \quad q = \frac{S-1}{2}N_y, \ldots, \frac{S+1}{2}N_y - 1, \\ 0, & \text{else}, \end{cases}$$

where $\rho_{pq} := \rho(x_p, y_q)$. Then we have

$$\widehat{\rho}(k_m, k_n) = \Delta x \Delta y \sum_{p=0}^{SN_x-1}\sum_{q=0}^{SN_y-1} \bar{\rho}_{pq} e^{-ik_m(x_p+SL)}e^{-ik_n(y_q+SL)},$$

where

$$k_m = \frac{\pi m}{SL}, \quad m = -\frac{SN_x}{2}, \ldots, \frac{SN_x}{2} - 1,$$
$$k_n = \frac{\pi n}{SL}, \quad n = -\frac{SN_y}{2}, \ldots, \frac{SN_y}{2} - 1,$$

$$x_p = -SL + p\left(\frac{2L}{N_x}\right), \quad p = 0, \ldots, SN_x - 1,$$
$$y_q = -SL + q\left(\frac{2L}{N_y}\right), \quad q = 0, \ldots, SN_y - 1.$$

Applying trapezoidal quadrature to (3.3), we approximate the values of φ as

$$\varphi(x_p, y_q) \approx \frac{1}{(2\pi)^2}\Delta k_x \Delta k_y \times \sum_{m=-\frac{SN_x}{2}}^{\frac{SN_x}{2}-1} \sum_{n=-\frac{SN_y}{2}}^{\frac{SN_y}{2}-1} \widehat{U}_G(k_m, k_n)\, \widehat{\rho}(k_m, k_n) e^{ik_m(x_p+SL)} e^{ik_n(y_q+SL)}. \tag{3.5}$$

The nonlocal interactions $\widehat{\chi}_j(\xi)$ defined by (1.12)-(1.13) consists of convolution and multiplication. Since the multiplication by the stationary state $\phi_s(\mathbf{x})$ and its conjugate can be easily determined, one has to efficiently compute the convolution $U*(\phi_s\xi)$. However, since $(\phi_s\xi)$ is smooth and fast-decaying, the KTM allows to accurately compute the corresponding convolution.

Thus the nonlocal interaction $\widehat{\chi}_j(\xi)$ can be efficiently computed in three steps — viz.

1. Multiply the ground state ϕ_s (or its conjugate) and function ξ.
2. Compute the convolution $\varphi := U*(\phi_s\xi)$ (or $\varphi := U*(\bar{\phi}_s\xi)$).
3. Multiply the convolution potential φ and the ground state ϕ_s.

Below, we present detailed step-by-step Algorithm 3.1 using $\widehat{\chi}_1(\xi)$ as an example. Its adaptation to $\widehat{\chi}_2(\xi)$ is obvious and direct.

Algorithm 3.1 KTM for computing $\widehat{\chi}_1(\xi)$

Require: Given a smooth function ξ, the ground state ϕ_s on mesh grid $\mathbb{T}_h$, pre-compute the Fourier transform $(\widehat{U}_G)_{mn}$.

1: Compute $\bar{\phi}_s\xi$ by multiplication.
2: Compute the density ρ by differentiating $\bar{\phi}_s\xi$ using Fourier spectral method.
3: Compute the Fourier transform of $\bar{\rho}_{pq}$ via FFT.
4: Compute $\widehat{\rho}_{mn}(\widehat{U}_G)_{mn}$ by multiplication.
5: Compute the potential φ (3.5) via inverse FFT.
6: Compute $\widehat{\chi}_1(\xi) = \phi_s\varphi$ by multiplication.

The following example shows the accuracy of Algorithm 3.1. For the sake of simplicity, we study the nonlocal interaction $\widehat{\chi}_1(\xi)$ as a representative.

Example 3.1. Consider $\phi_s(\mathbf{x}) = e^{-|\mathbf{x}|^2/2\sigma^2}$ and $\xi(\mathbf{x}) = \phi_s(\mathbf{x})$. The computational domain $\Omega := [-12, 12]^2$ is discretised uniformly in each direction with the mesh of size h. As the reference solutions we take the numerical one on the fine mesh with size $h = 1/16$.

Table 1: Example 3.1. Accuracy of nonlocal interaction $\widehat{\chi}_1(\xi)$, $\sigma = 2$, $\gamma = 32$.

h	2	1	1/2	1/4
$\mathbf{n} = (0,0,1)^T$	1.5975E-02	1.1291E-06	1.4544E-15	1.8422E-15
$\mathbf{n} = (1,0,0)^T$	1.5975E-02	1.1574E-06	1.3574E-15	1.3574E-15
$\mathbf{n} = (\frac{\sqrt{6}}{3}, \frac{\sqrt{3}}{3}, 0)^T$	1.4624E-02	2.4054E-06	1.0665E-15	1.5513E-15
$\mathbf{n} = (0, \frac{\sqrt{6}}{3}, \frac{\sqrt{3}}{3})^T$	2.5869E-02	5.7621E-06	3.2386E-15	4.2737E-15

Table 1 shows the accuracy in relative maximum norm of the nonlocal interaction $\widehat{\chi}_1(\xi)$ for different mesh sizes h and different dipolar orientations $\mathbf{n}$. Note that the numerical errors of the nonlocal interaction $\widehat{\chi}_1(\xi)$ have the spatial spectral accuracy.

3.3. Numerical computation for BdG equations

In order to accelerate the solution of the eigenvalue problem (2.9), we will employ a multigrid method — cf. Algorithm 3.2. First, we generate an initial mesh grid $\mathscr{T}_{h_1}$ with mesh size h_1 and consider the $\mathscr{T}_{h_{k+1}}$ obtained from $\mathscr{T}_{h_k}$ $(k = 1, 2, \ldots, n)$ by regular refinements such that $h_{k+1} = h_k/2$. Let $\mathbf{I}_{h_k}^{h_{k+1}}$ refer to the Fourier spectral interpolation operator from $\mathscr{T}_{h_k}$ to $\mathscr{T}_{h_{k+1}}$. The process of solving (3.1) by IRAM is denoted by

$$\left(f^{h_k}, \omega^{h_k}\right) = \texttt{IRAM}\left(\hat{f}^{h_k}, \mathscr{T}_{h_k}\right),$$

where $\hat{f}^{h_k}$ is the initial value, $\mathscr{T}_{h_k}$ the k-th mesh grid and (f^{h_k}, ω^{h_k}) the solution.

Algorithm 3.2 Multigrid method for eigenvalue problem

Require: Given a initial mesh grid $\mathscr{T}_{h_1}$ and initial value $\hat{f}^{h_1}$ of the initial mesh $\mathscr{T}_{h_1}$ randomly.

1: Use Fourier spectral method and Algorithm 3.1 to discretise (2.9) and obtain (3.1).
2: Solve $(f^{h_1}, \omega^{h_1}) = \texttt{IRAM}(\hat{f}^{h_1}, \mathscr{T}_{h_1})$ to obtain (f^{h_1}, ω^{h_1}), and set $k = 1$.
3: For $k = 1, \ldots, n-1$, do the following iteration

- Set $\hat{f}^{h_{k+1}} = \mathbf{I}_{h_k}^{h_{k+1}} f_{h_k}$.
- Use Fourier spectral method and Algorithm 3.1 to discretise (2.9) and obtain (3.1).
- Do the solving process $(f^{h_{k+1}}, \omega^{h_{k+1}}) = \texttt{IRAM}(\hat{f}^{h_{k+1}}, \mathscr{T}_{h_k})$.

End Do

Remark 3.1. Since the corresponding linear system (3.1) is non-symmetric, real-valued and dense, it is impossible to explicitly store the corresponding large matrix because of memory constraints. It is necessary to utilise the matrix-free version of the IRAM. In this work, we only have to provide the operator-function action — i.e. to compute $z \leftarrow H_h^- H_h^+ \xi$ for a given ξ, which is updated iteratively to approximate the eigenfunction.

The next algorithm is used for solving the BdG equations (1.9)-(1.10).

Algorithm 3.3 Main method for BdG equations

1: Compute the stationary state ϕ_s and chemical potential μ_s in (1.6) for quasi-2D model by PCG-KTM.
2: Solve the fourth order linear nonsymmetric eigenvalue problem (2.9) by Algorithm 3.2 to compute the first k smallest magnitude eigenvalues ω_ℓ^h, $\ell = 1,\ldots,k$ and the corresponding eigenfunctions f_ℓ^h, $\ell = 1,\ldots,k$ on the bounded domain Ω.
3: Evaluate (2.7) to obtain g_ℓ^h, $\ell = 1,\ldots,k$.
4: Based on (2.2), we can obtain normalised numerical solutions (u_ℓ^h, v_ℓ^h), $\ell = 1,\ldots,k$ corresponding to eigenvalue ω_ℓ^h, $\ell = 1,\ldots,k$ by using the discrete normalisation conditions (2.6) of f and g .

4. Numerical Results

Let us consider numerical examples in order to illustrate the accuracy and effectiveness of the methods introduced in Section 3. In Subsection 4.1, we study the influence of different harmonic potentials and dipolar orientation on Bogoliubov excitations around the ground state of GPE. Computing the ground state solution of the BEC and eigenpairs of BdG equations, we check the accuracy of numerical method and validity of our analysis. The efficiency of the multigrid method is considered in Subsection 4.2. Subsection 4.3 is devoted to the convergence of the BdG equation for quasi-2D and limit model. In Subsection 4.4, we present a few interesting phenomena related to the BdG excitations of quasi-2D dipolar BEC from the eigenvalue coincidence, pairing and crossing. We also show interesting effects of the BdG excitations of quasi-2D dipolar BEC in Subsection 4.4.

The exact ground state ϕ_g is computed numerically by the PCG-KTM algorithm [4] on a large enough domain by using a fine mesh size h such that the errors of the spatial discretisation is negligible. The BdG equation is solved on $\mathcal{T}_h$ where the numerical ground state ϕ_g^h is interpolated by the Fourier spectral method from the exact solution ϕ_g. The algorithms were implemented in MATLAB R2019b, and run on a 2.27GH Intel(R) Xeon(R) CPU E5520 with a 8 MB cache in Debian GNU/Linux. We adapt matrix-free version `eigs` function in MATLAB to solve large-scale, dense and nonsymmetric algebraic eigenvalue problems.

4.1. Accuracy tests

Here, we demonstrate the numerical spectral accuracy confirmation by employing a harmonic trap. Since we have obtained exact solution ϕ_g, Lemma 2.2 allows to determine obtain analytical solutions $(\omega_\ell, u_\ell, v_\ell)$, $\ell = 1,2$ of the BdG equations (1.9)-(1.10) for the harmonic potential $V(x,y)$.

Using a reference solution, we define the relative error of numerical solutions $(\omega_\ell^h, u_\ell^h, v_\ell^h)$ $(\ell = 1,2)$ by

$$\varepsilon^h_{\omega_\ell} = |\omega_\ell - \omega^h_\ell|, \quad \varepsilon^h_{\mathrm{fun}_\ell} = \varepsilon^h_{u_\ell} + \varepsilon^h_{v_\ell},$$

where

$$\varepsilon^h_{u_\ell} = \frac{\|u^h_\ell - u_\ell\|_{l^2}}{\|u^h_\ell\|_{l^2}}, \quad \varepsilon^h_{v_\ell} = \frac{\|v^h_\ell - v_\ell\|_{l^2}}{\|v^h_\ell\|_{l^2}}.$$

Example 4.1. For harmonic potential $V(x,y) = (\gamma_x^2 x^2 + \gamma_y^2 y^2)/2$, computational domain $\Omega = [-12,12]^2$, and the initial mesh size $h_0 = 1$, we consider two cases.

Case 1. $\gamma_x = \gamma_y = 1$ (symmetric trap), $\beta = 200, \lambda = 50$, $\varepsilon = 1/\sqrt{10}$, and $\mathbf{n} = (1,0,0)^T$, $\mathbf{n} = (\sqrt{6}/3, \sqrt{3}/3, 0)^T$ or $\mathbf{n} = (\sqrt{3}/3, \sqrt{3}/3, \sqrt{3}/3)^T$.

Case 2. $\gamma_x = 1, \gamma_y = 2$ (asymmetric trap), $\beta = 150, \lambda = -50$, $\varepsilon = 1/\sqrt{32}$, and $\mathbf{n} = (0,0,1)^T$, $\mathbf{n} = (\sqrt{2}/2, 0, \sqrt{2}/2)^T$ or $\mathbf{n} = (1/2, 1/2, \sqrt{2}/2)^T$.

In Case 1, the eigenvalues are $\omega_x = \omega_y = 1$ and the dimension of the eigenvspace is two. In Case 2, $\omega_x = 1$ and $\omega_y = 2$, thus the corresponding eigenspaces have dimension one.

The exact ground state ϕ_g is computed on $\Omega = [-12,12]^2$ with mesh size $h = 1/16$. The BdG equation is solved numerically on the same domain with the residual accuracy tolerance 10^{-10} and 10^{-9} for the symmetric and asymmetric traps, respectively. Table 2 shows that for different dipole orientations $\mathbf{n}$, the numerical errors have spatial spectral accuracy .

4.2. Efficiency of the multigrid method

Consider the efficiency of Algorithm 3.2.

Example 4.2. For harmonic potential $V(x,y) = (\gamma_x^2 x^2 + \gamma_y^2 y^2)/2$, computational domain $\Omega = [-12,12]^2$, and the initial mesh size $h_0 = 3/4$, we study two cases

Case 1. $\gamma_x = \gamma_y = 1$ (symmetric trap), $\beta = 200, \lambda = 50$, $\varepsilon = 1/\sqrt{10}$, and $\mathbf{n} = (1,0,0)^T$.

Case 2. $\gamma_x = 1, \gamma_y = 2$ (asymmetric trap), $\beta = 150, \lambda = -50$, $\varepsilon = 1/\sqrt{32}$, and $\mathbf{n} = (0,0,1)^T$.

The initial values of the direct method are selected by the default random selection of MATLAB. For the initial mesh $\mathcal{T}_{h_0}$, we choose the same initial values as in Algorithm 3.2. Table 3 shows that for eigenvalue problems, the multigrid method more very efficient than the direct one.

4.3. Asymptotic convergence for quasi-2D and limit model

The example below deals with the asymptotic convergence of the BdG equations for quasi-2D and limit models.

Table 2: Example 4.1. Numerical errors for the BdG equation.

Case 1: $\gamma_x = 1, \quad \gamma_y = 1$					
	h	$h_0 = 1$	$h_0/2$	$h_0/4$	$h_0/8$
$\vec{n} = (1,0,0)$	$\varepsilon^h_{\omega_1}$	1.291E-02	2.481E-05	8.894E-08	6.933E-10
	$\varepsilon^h_{\omega_2}$	1.935E-03	8.339E-06	9.665e-08	7.483E-10
	$\varepsilon^h_{\text{fun}_1}$	4.781E-02	9.994E-04	9.195E-08	3.229E-10
	$\varepsilon^h_{\text{fun}_2}$	4.109E-02	4.759E-04	3.701E-07	3.783E-10
$\vec{n} = \left(\frac{\sqrt{6}}{3}, \frac{\sqrt{3}}{3}, 0\right)$	$\varepsilon^h_{\omega_1}$	1.109E-02	2.644E-05	1.996E-08	1.113E-10
	$\varepsilon^h_{\omega_2}$	7.147E-03	1.256E-05	2.175E-08	1.440E-10
	$\varepsilon^h_{\text{fun}_1}$	4.551E-02	8.466E-04	2.107E-07	1.480E-10
	$\varepsilon^h_{\text{fun}_2}$	4.355E-02	6.519E-04	2.366E-07	1.816E-10
$\vec{n} = \left(\frac{\sqrt{3}}{3}, \frac{\sqrt{3}}{3}, \frac{\sqrt{3}}{3}\right)$	$\varepsilon^h_{\omega_1}$	2.564E-03	3.711E-06	2.671E-08	1.616E-11
	$\varepsilon^h_{\omega_2}$	1.825E-05	5.267E-06	2.848E-08	1.717E-11
	$\varepsilon^h_{\text{fun}_1}$	4.536E-02	5.185E-04	1.170E-07	1.916E-10
	$\varepsilon^h_{\text{fun}_2}$	4.343E-02	5.278E-04	1.136E-07	2.979E-10
Case 2: $\gamma_x = 1, \quad \gamma_y = 2$					
	h	$h_0 = 1$	$h_0/2$	$h_0/4$	$h_0/8$
$\vec{n} = (0,0,1)$	$\varepsilon^h_{\omega_1}$	1.082E-01	1.346E-03	1.863E-06	2.971E-09
	$\varepsilon^h_{\omega_2}$	1.622E-01	9.422E-04	9.605e-07	1.484E-10
	$\varepsilon^h_{\text{fun}_1}$	8.288E-02	1.513E-03	1.306E-06	1.410E-09
	$\varepsilon^h_{\text{fun}_2}$	2.817E-01	1.085E-02	3.527E-05	2.064E-09
$\vec{n} = \left(\frac{\sqrt{2}}{2}, 0, \frac{\sqrt{2}}{2}\right)$	$\varepsilon^h_{\omega_1}$	3.991E-02	6.424E-04	9.941E-07	1.384E-09
	$\varepsilon^h_{\omega_2}$	2.008E-01	6.107E-04	5.402E-07	4.816E-10
	$\varepsilon^h_{\text{fun}_1}$	7.692E-02	9.285E-04	6.781E-07	1.027E-09
	$\varepsilon^h_{\text{fun}_2}$	3.532E-01	1.007E-02	2.778E-05	4.308E-09
$\vec{n} = \left(\frac{1}{2}, \frac{1}{2}, \frac{\sqrt{2}}{2}\right)$	$\varepsilon^h_{\omega_1}$	8.319E-03	9.876E-04	5.630E-08	3.825E-10
	$\varepsilon^h_{\omega_2}$	1.873E-01	4.055E-04	3.914E-08	1.112E-10
	$\varepsilon^h_{\text{fun}_1}$	7.766E-02	9.894E-04	4.914E-07	3.227E-10
	$\varepsilon^h_{\text{fun}_2}$	3.541E-01	9.829E-03	1.647E-05	5.879E-10

Example 4.3. For harmonic potential $V(x,y) = (\gamma_x^2 x^2 + \gamma_y^2 y^2)/2$, computational domain $\Omega = [-12,12]^2$ and the mesh size $h = 1/8$, we study two cases.

Case 1. $\gamma_x = 1, \gamma_y = 1$, $\beta = 250, \lambda = 100$, $\mathbf{n} = (1,0,0)^T$, and change ϵ from $1/2^0$ to $1/2^{10}$.

Case 2. $\gamma_x = 1, \gamma_y = 3$, $\beta = 180, \lambda = 60$, $\mathbf{n} = (\sqrt{2}/2, \sqrt{2}/2, 0)^T$, and change ϵ from $1/2^0$ to $1/2^{10}$.

Table 3: Example 4.2. Number of iterations.

Case I: $\gamma_x = 1, \quad \gamma_y = 1$				
	$h_0 = 3/4$	$h_1 = h_0/2$	$h_1 = h_0/4$	$h_1 = h_0/8$
Multigrid method	87	132	323	1370
Direct method	87	140	497	3042
Case II: $\gamma_x = 1, \quad \gamma_y = 2$				
	$h_0 = 3/4$	$h_1 = h_0/2$	$h_1 = h_0/4$	$h_1 = h_0/8$
Multigrid method	219	244	397	1137
Direct method	219	268	556	2964

In the limit case, we solve the BdG equations with the limit dipole convolution kernel $U^{\infty}(\mathbf{x}) := (1/2\pi)(1/|\mathbf{x}|)$ and obtain eigenpairs $(\omega_l^{\infty}, u_\ell^{\infty}, v_\ell^{\infty})$, $\ell = 1, 2, \ldots$. Lemma 2.2 yields that the first or the second eigenpair does not depend on ϵ, so that we do not have to compare the errors for the first and the second eigenpairs. Let us set

$$\varepsilon_{\omega_\ell} = |\omega_\ell^{\infty} - \omega_\ell|, \quad \varepsilon_{u_\ell} = \frac{\|u_\ell^{\infty} - u_\ell\|_{l^2}}{\|u_\ell\|_{l^2}}, \quad \varepsilon_{v_\ell} = \frac{\|v_\ell^{\infty} - v_\ell\|_{l^2}}{\|v_\ell\|_{l^2}}. \tag{4.1}$$

The numerical results for eigenpair approximations presented in Fig. 1, show that our method can achieve optimal first convergence order — cf. [7].

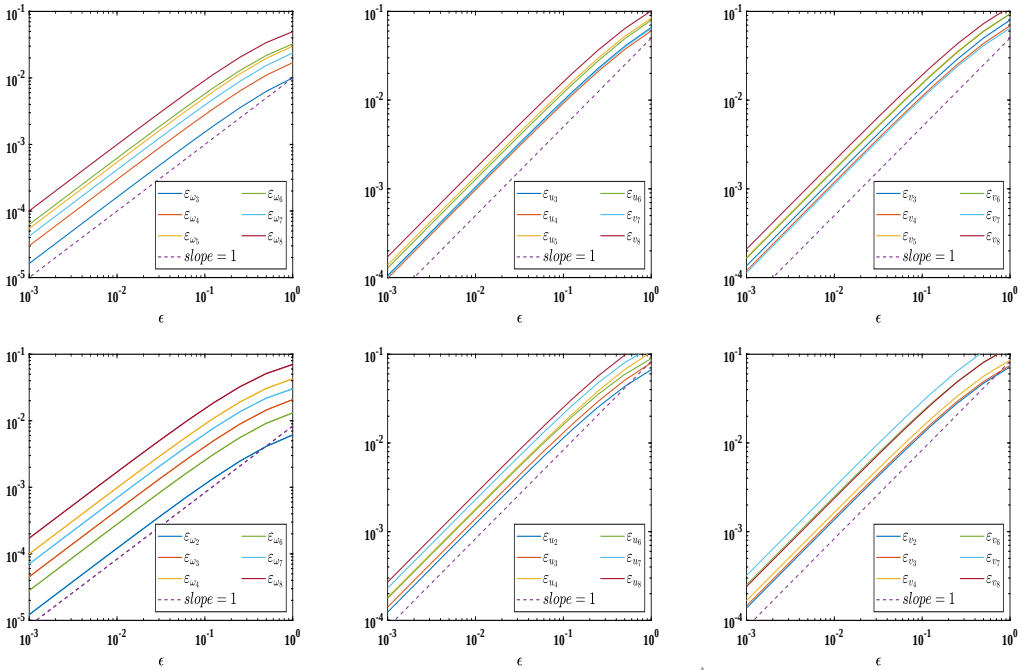

Figure 1: Example 4.3. Errors. Top Row: Case 1. Bottom Row: Case 2. Left: ω_ℓ. Middle: u_ℓ. Right: v_ℓ.

4.4. BdG solutions of dipolar BECs

Example 4.4. For harmonic potential $V(x,y) = (\gamma_x^2 x^2 + \gamma_y^2 y^2)/2$, $\mathbf{n} = (0,0,1)^T$, computational domain $\Omega = [-12,12]^2$, and the mesh size $h = 1/8$, we consider three cases.

Case 1. $\gamma_x = 1, \gamma_y = 1$, fixed $\beta = 250$, $\epsilon = 1/\sqrt{10}$, change λ from -100 to 80.

Case 2. $\gamma_x = 1, \gamma_y = 1$, fixed $\lambda = -100$, $\epsilon = 1/\sqrt{24}$, change β from 0 to 200.

Case 3. $\gamma_x = 1, \gamma_y = 1$, fixed $\beta = 150$, $\lambda = -50$, change ϵ from $1/1024$ to 1.

Fig. 2 shows the eigenvalues ω_ℓ, $\ell = 1, \cdots, 9$ for $\beta = 250$, $\epsilon = \frac{1}{\sqrt{10}}$, different λ on the left (Case 1) and $\lambda = -100$, $\epsilon = \frac{1}{\sqrt{24}}$, different β on the middle (Case 2) and $\beta = 150$, $\lambda = -50$, different ϵ on the right (Case 3). In Case 1-3, the lowest eigenvalue $\omega_1 = \omega_2 = 1$ remains the same. This indicates that in an external harmonic potential corresponding to a rigid motion of the center of mass, the lowest dipole mode does not depend on the nature of the interatomic forces [20, 39]. The associated numerical amplitudes for $\omega_1 = \omega_2 = 1$, presented in Fig. 2, are consistent with the analytical solutions in Lemma 2.2. Moreover, we observe that the multiplicity of eigenvalue ω_7 is 1, while $\omega_1 = \omega_2$, $\omega_3 = \omega_4$, $\omega_5 = \omega_6$ and $\omega_8 = \omega_9$, which indicates that the multiplicity of eigenvalues ω_1, ω_3, ω_5 and ω_8 is two.

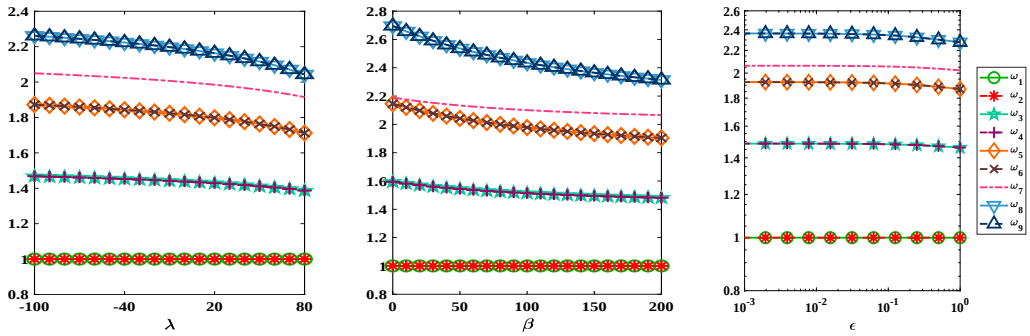

Figure 2: Example 4.4. Eigenvalues ω_ℓ, $\gamma_x = \gamma_y = 1$, $\mathbf{n} = (0,0,1)$. Left: $\beta = 250$, $\epsilon = 1/\sqrt{10}$ (Case 1). Middle: $\lambda = -100$, $\epsilon = 1/\sqrt{24}$ (Case 2). Right: $\beta = 150$, $\lambda = -50$ (Case 3).

Example 4.5. In this example, we consider the harmonic potentials $V(x,y) = (\gamma_x^2 x^2 + \gamma_y^2 y^2)/2$, $\mathbf{n} = (1,0,0)^T$, computational domain $\Omega = [-12,12]^2$, mesh size $h = 1/8$.

Case 1. $\gamma_x = 1, \gamma_y = 4$, fixed $\beta = 200$, $\epsilon = 1/\sqrt{60}$, change λ from 0 to 200.

Case 2. $\gamma_x = 1, \gamma_y = 4$, fixed $\lambda = 40$, $\epsilon = 1/\sqrt{120}$, change β from 0 to 200.

Case 3. $\gamma_x = 1, \gamma_y = 4$, fixed $\beta = 250$, $\lambda = 100$, change ϵ from $1/1024$ to 1.

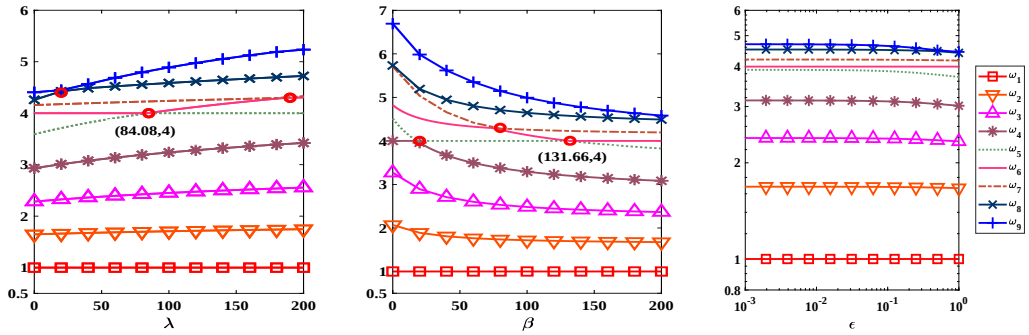

Figure 3: Example 4.5. Eigenvalues ω_ℓ, $\gamma_x = 1$, $\gamma_y = 4$, $\mathbf{n} = (1,0,0)$. Left: $\beta = 200$, $\epsilon = 1/\sqrt{60}$ (Case 1). Middle: $\lambda = 40$, $\epsilon = 1/\sqrt{120}$ (Case 2). Right: $\beta = 250$, $\lambda = 100$ (Case 3).

Fig. 3 shows the eigenvalues ω_ℓ, $\ell = 1,\ldots,9$ for $\beta = 100$, $\epsilon = 1/4$, different λ in the left (Case 1) and $\lambda = 40$, $\epsilon = 1/\sqrt{120}$, different β in the middle (Case 2), and $\beta = 250$, $\lambda = 100$, different ϵ in the right (Case 3). For Cases 1-3, the associated numerical amplitudes for $\omega_1 = 1$ and 4 presented in Fig. 3, are consistent with the analytical solutions in Lemma 2.2. Fig. 3 indicates that the multiplicities of all of eigenvalues ω_ℓ, $\ell = 1,\ldots,9$ are single. The eigenvalue 4 remains unchanged but its order can change: ω_6 changes to ω_5 (left) and ω_4 changes to ω_5 change to ω_6 (right). We choose two from all of intersection points. The intersection point in Case I is around 80.08, and the intersection point in Case II is around 131.66 (up to two decimal places). The intersection point means the multiplicity of the eigenvalue is two.

Example 4.6. For harmonic potential $V(x,y) = (\gamma_x^2 x^2 + \gamma_y^2 y^2)/2$, $\beta = 200$, $\lambda = 100$, $\epsilon = 1/4$, computational domain $\Omega = [-12,12]^2$ and the mesh size $h = 1/8$, we consider three cases.

Case 1. $\gamma_x = \gamma_y = 1$, $\mathbf{n} = (0,1,0)^T$.

Case 2. $\gamma_x = \gamma_y = 1$, $\mathbf{n} = (\sqrt{6}/3, \sqrt{3}/3, 0)^T$.

Case 3. $\gamma_x = 1$, $\gamma_y = 3$, $\mathbf{n} = (0,1,0)^T$.

Fig. 4, containing the contour plots of numerical solutions (u_ℓ, v_ℓ), shows that the dipole orientation essentially affects the eigenmodes (u_ℓ, v_ℓ). The eigenmodes (u_ℓ, v_ℓ) orientations are parallel to the dipole orientation. It also indicates that the influence of anisotropic external potential ($\gamma_y > \gamma_x$) on the eigenmodes is also very significant. Indeed, the presence of DDI and anisotropic external potential leads to a much richer phase diagram for eigenmodes of the BdG equations.

5. Conclusion

We propose an efficient spectrally accurate multigrid method for the BdG excitations of the quasi-2D dipolar BECs. The wave function/eigenmodes are spatially discretised by

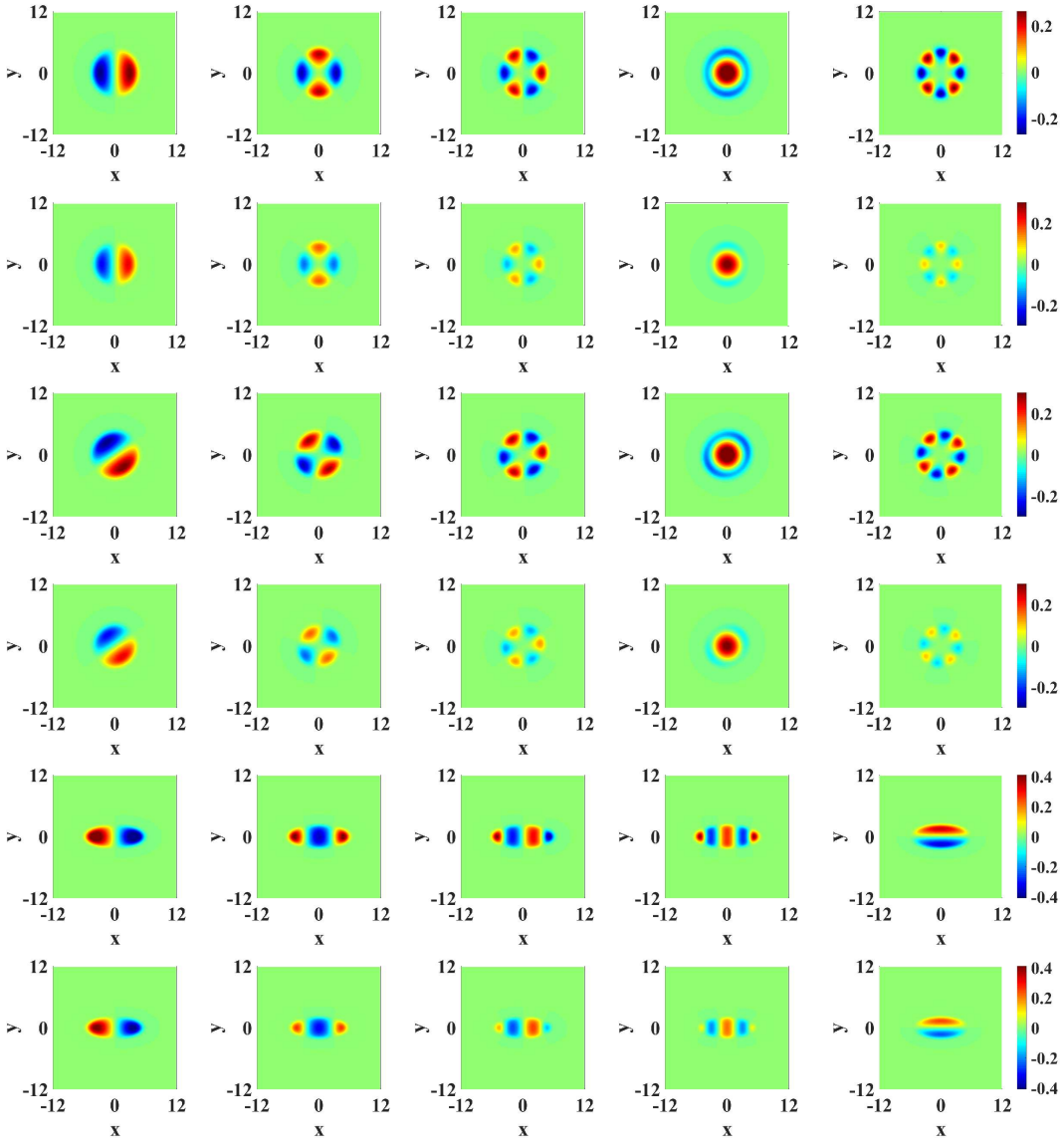

Figure 4: Example 4.6. Contour plots of eigenmodes. Rows 1-2: Case 1. Rows 3-4: Case 2. Rows 5-6: Case 3. Even rows: $u_1, \ldots, u_5$ from left to right. Odd rows: $v_1, \ldots, v_5$ from left to right.

the Fourier spectral method. The convolution-type nonlocal potential can be computed in $\mathcal{O}(N \log(N))$ operations with a spectral accuracy by KTM. Non-symmetric and dense eigenvalue system are solved by the matrix free version of IRAM. Examples confirm the spectral accuracy of the method. Besides, the influence of the model parameters on the eigenvalue distribution is studied and for various dipole orientations and an anisotropic external potential the phase diagrams of the eigenmodes is presented. The method can be extended to other problems such as BdG equation for rotating BEC, high-order local interaction, multi-component BECs.

Acknowledgments

The authors would like to thank Prof. Yong Zhang (Tianjin University) for his stimulating discussions and fruitful cooperations that have motivated this work. This work was supported in part by the National Natural Science Foundation of China (Grant Nos. 12001402, 12071343).

References

[1] K. Aikawa, A. Frisch, M. Mark, S. Baier, A. Rietzler, R. Grimm and F. Ferlaino, *Bose-Einstein Condensation of Erbium*, Phys. Rev. Lett. **108**, Article 210401 (2012).

[2] M.H. Anderson, J.R. Ensher, M.R. Matthews, C.E. Wieman, and E.A. Cornell, *Observation of Bose-Einstein condensation in a dilute atomic vapor*, Science **269**, 198–201 (1995).

[3] X. Antoine, A. Levitt, and Q. Tang, *Efficient spectral computation of the stationary states of rotating Bose-Einstein condensates by the preconditioned nonlinear conjugate gradient method*, J. Comput. Phys. **343**, 92–109 (2017).

[4] X. Antoine, Q. Tang, and Y. Zhang, *A preconditioned conjugated gradient method for computing ground sates of rotating dipolar Bose-Einstein condensates via kernel truncation method for dipole-dipole interaction evaluation*, Commun. Comput. Phys. **24** (4), 966–988 (2018).

[5] D. Baillie, R.M. Wilson, and P.B. Blakie, *Collective excitations of self-bound droplets of a dipolar quantum fluid*, Phys. Rev. Lett. **119** (25), Article 255302 (2017).

[6] W. Bao, N.B. Abdallah, and Y. Cai, *Gross-Pitaevskii-Poisson equations for dipolar Bose-Einstein condensate with anisotropic confinement*, SIAM J. Math. Anal. **44**, 1713–1741 (2012).

[7] W. Bao and Y. Cai, *Mathematical theory and numerical methods for Bose-Einstein condensation*, Kinet. Relat. Mod. **6** (1), 1–135 (2013).

[8] W. Bao and Y. Cai, *Mathematical models and numerical methods for spinor Bose-Einstein condensates*, Commun. Comput. Phys. **24**, 899–965 (2018).

[9] W. Bao, Y. Cai, and H. Wang, *Efficient numerical methods for computing ground states and dynamics of dipolar Bose-Einstein condensates*, J. Comput. Phys. **229**, 7874–7892 (2010).

[10] W. Bao and Q. Du, *Computing the ground state solution of Bose-Einstein condensates by a normalized gradient flow*, SIAM J. Sci. Comput. **25** (5), 1674–1697 (2004).

[11] W. Bao, H. Jian, N.J. Mauser, and Y. Zhang, *Dimension reduction of the Schrödinger equation with coulomb and anisotropic confining potentials*, SIAM J. Appl. Math. **73** (6), 2100–2123 (2013).

[12] W. Bao, D. Marahrens, Q. Tang and Y. Zhang, *A simple and efficient numerical method for computing the dynamics of rotating dipolar Bose-Einstein condensates via rotating Lagrangian coordinates*, SIAM J. Sci. Comput. **35**, A2671–A2695 (2013).

[13] W. Bao, Q. Tang, and Y. Zhang, *Accurate and efficient numerical methods for computing ground states and dynamics of dipolar Bose-Einstein condensates via the nonuniform FFT*, Commun. Comput. Phys. **19** (5), 1141–1166 (2016).

[14] C.C. Bradley, C.A. Sackett, J.J. Tollett, and R.G. Hulet, *Evidence of Bose-Einstein condensation in an atomic gas with attractive interactions*, Phys. Rev. Lett. **75**, 1687–1690 (1995).

[15] R. Carles, P.A. Markowich and C. Sparber, *On the Gross-Pitaevskii equation for trapped dipolar quantum gases*, Nonlinearity **21**, 2569–2590 (2008).

[16] F. Dalfovo, S. Giorgini, L. Pitaevskii, and S. Stringari, *Theory of Bose-Einstein condensation in trapped gases*, Rev. Mod. Phys. **71** (3), 463–512 (1999).

[17] I. Danaila and F. Hecht, *A finite element method with mesh adaptivity for computing vortex states in fast-rotating Bose-Einstein condensates*, J. Comput. Phys. **229**, 6946–6960 (2010).
[18] I. Danaila, M.A. Khamehchi, V. Gokhroo, P. Engels, and P.G. Kevrekidis, *Vector dark-antidark solitary waves in multicomponent Bose-Einstein condensates*, Phys. Rev. A **94** (5), Article 053617 (2016).
[19] K.B. Davis, M.-O. Mewes, M.R. Andrews, N.J. van Druten, D.S. Durfee, D.M. Kurn, and W. Ketterle, *Bose-Einstein condensation in a gas of sodium atoms*, Phys. Rev. Lett. **75**, 3969–3973 (1995).
[20] M. Edwards, P.A. Ruprecht, K. Burnett, R.J. Dodd, and C.W. Clark, *Collective excitations of atomic Bose-Einstein condensates*, Phys. Rev. Lett. **77** (9), 1671–1674 (1996).
[21] L. Exl, N.J. Mauser and Y. Zhang, *Accurate and efficient computation of nonlocal potentials based on Gaussian-sum approximation*, J. Comput. Phys. **327**, 629–642 (2016).
[22] A.L. Fetter, *Rotating trapped Bose-Einstein condensates*, Rev. Mod. Phys. **81**, 647–691 (2009).
[23] Y. Gao and Y. Cai, *Numerical methods for Bogoliubov-de Gennes excitations of Bose-Einstein condensates*, J. Comput. Phys. **403**, Article 109058 (2020).
[24] K. Gòral, K. Rzazewski and T. Pfau, *Bose-Einstein condensation with magnetic dipole-dipole forces*, Phys. Rev. A **61**, Article 051601 (2000).
[25] L. Greengard, S. Jiang and Y. Zhang, *The anisotropic truncated kernel method for convolution with free-space Green's functions*, SIAM J. Sci. Comput. **40**(6), A3733–A3754 (2018).
[26] A. Griesmaier, J. Werner, S. Hensler, J. Stuhler, and T. Pfau, *Bose-Einstein condensation of Chromium*, Phys. Rev. Lett. **94**, Article 160401 (2005).
[27] B. Hu, G. Huang, and Y.L. Ma, *Analytical solutions of the Bogoliubov-de Gennes equations for excitations of a trapped Bose-Einstein-condensed gas*, Phys. Rev. A **69** (6), Article 063608 (2004).
[28] Z. Huang, P.A. Markowich and C. Sparber, *Numerical simulation of trapped dipolar quantum gases: collapse studies and vortex dynamics*, Kinet. Relat. Mod. **3**, 181–194 (2010).
[29] L. Jia, A.-B. Wang, and S. Yi, *Low-lying excitations of vortex lattices in condensates with anisotropic dipole-dipole interaction*, Phys. Rev. A **97**, Article 043614 (2018).
[30] S. Jia, H. Xie, M. Xie and F. Xu, *A full multigrid method for nonlinear eigenvalue problems*, Sci. China Math. **59** (10), 2037–2048 (2016).
[31] T.F. Jiang, W.C. Su, *Ground state of the dipolar Bose-Einstein condensate*, Phys. Rev. A **74**, Article 063602 (2006).
[32] H. Kadau, M. Schmitt, M. Wenzel, C. Wink, T. Maier, I. Ferrier-Barbut, and T. Pfau, *Observing the Rosensweig instability of a quantum ferrofluid*, Nature **530**, 194–197 (2016).
[33] A.J. Leggett, *Bose-Einstein condensation in the alkali gases: Some fundamental concepts*, Rev. Mod. Phys. **73** (2), 307–356 (2001).
[34] N.G. Parker, C. Ticknor, A.M. Martin and D.H. O'Dell, *Structure formation during the collapse of a dipolar atomic Bose-Einstein condensate*, Phys. Rev. A **79**, Article 013617 (2009).
[35] S. Ronen, D.C. Bortolotti and J.L. Bohn, *Bogoliubov modes of a dipolar condensate in a cylindrical trap*, Phys. Rev. A **74**, Article 013623 (2006).
[36] C.A. Rozzi, D. Varsano, A. Marini, E.K. Gross, and A. Rubio, *Exact coulomb cutoff technique for supercell calculations*, Phys. Rev. B **73** (20), Article 205119 (2006).
[37] Y. Saad, *Numerical methods for large eigenvalue problems*, SIAM (2011).
[38] L. Santos, G.V. Shlyapnikov, P. Zoller and M. Lewenstein, *Bose-Einstein condensation in trapped dipolar gases*, Phys. Rev. Lett. **85**, 1791–1794 (2000).
[39] S. Stringari, *Collective excitations of a trapped Bose-condensed gas*, Phys. Rev. Lett. **77** (12), 2360–2363 (1996).
[40] F. Vico, L. Greengard, and M. Ferrando, *Fast convolution with free-space functions*, J. Comput. Phys. **323**, 191–203 (2016).

[41] R.M. Wilson and S. Ronen and J.L. Bohn, *Stability and excitations of a dipolar Bose-Einstein condensate with a vortex*, Phys. Rev. A **79**, Article 013621 (2009).
[42] H. Xie and M. Xie, *A multigrid method for ground state solution of Bose-Einstein condensates*, Commun. Comput. Phys. **19** (3), 648–662 (2016).
[43] S. Yi and L. You, *Trapped condensates of atoms with dipole interactions*, Phys. Rev. A **63**, Article 053607 (2001).
[44] Y. Yuan, Z. Xu, Q. Tang and H. Wang, *The numerical study of the ground states of spin-1 Bose-Einstein condensates with spin-orbit-coupling*, East Asian J. Appl. Math. **8**, 598–610 (2018).